UC Berkeley
UC Berkeley Previously Published Works

Title
Adaptive optical microscopy for neurobiology

Permalink
https://escholarship.org/uc/item/8xg2p279

Authors
Rodríguez, Cristina
Ji, Na

Publication Date
2018-06-01

DOI
10.1016/j.conb.2018.01.011

Peer reviewed

Adaptive optical microscopy for neurobiology

Cristina Rodríguez[1] and **Na Ji**[1,2]

[1]Janelia Research Campus, Howard Hughes Medical Institute, Ashburn, VA 20147, USA

[2]Department of Physics, Department of Molecular & Cellular Biology, University of California, Berkeley, CA 94720, USA

Abstract

With the ability to correct for the aberrations introduced by biological specimens, adaptive optics — a method originally developed for astronomical telescopes — has been applied to optical microscopy to recover diffraction-limited imaging performance deep within living tissue. In particular, this technology has been used to improve image quality and provide a more accurate characterization of both structure and function of neurons in a variety of living organisms. Among its many highlights, adaptive optical microscopy has made it possible to image large volumes with diffraction-limited resolution in zebrafish larval brains, to resolve dendritic spines over 600 μm deep in the mouse brain, and to more accurately characterize the orientation tuning properties of thalamic boutons in the primary visual cortex of awake mice.

Introduction

Optical microscopy has allowed the discovery of physical structures and phenomena otherwise invisible or unresolvable to our bare eyes. A wide variety of disciplines have greatly benefited from this centuries old methodology. In particular, the field of modern neuroscience is based on Ramón y Cajal's identification of neurons as the elementary computational unit of the brain using optical microscopes.

Because of the wave nature of light, the resolution of conventional optical microscopes is limited by diffraction to approximately half the wavelength of light. In practice, however, optimal performance of microscopes is achievable only under rather limited conditions, requiring specific coverglass thickness and immersion medium for the objective. Additionally, the optical properties of the specimen and the immersion medium need to be matched. The latter is seldom achieved for most biological samples, whose very own mixture of ingredients (e.g. water, proteins, nuclear acids, and lipids) gives rise to spatial variations in the refractive index. Such inhomogeneities induce wavefront aberrations, leading to a degradation in the resolution and contrast of microscope images that further deteriorates with imaging depth.

Corresponding author: Ji, Na (jin@janelia.hhmi.org).

By dynamically measuring the accumulated distortion of light as it travels through inhomogeneous specimens, and correcting for it using active optical components, adaptive optics (AO) can recover diffraction-limited performance deep within living systems. In the present review, we outline the fundamental concepts and methods of adaptive optical microscopy, highlighting recent applications of this technology to neurobiology. As opposed to other schemes that target the scattered light [1–3], this review focuses on approaches that act on the focus-forming ballistic light and correct for lower order aberrations. For a more in-depth examination on adaptive optical microscopy applications, methods, and implementations, we direct the reader to other comprehensive sources [4–7].

Adaptive optics in microscopy

To recover ideal imaging performance, AO methods measure the distorted wavefront(s) involved in image formation, and modify the wavefront accordingly to compensate for such aberrations (Figure 1), which can be introduced by the sample [8,9] or intrinsic to the optical system. Detecting the presence of aberrations in a microscope can be done by measuring its point-spread function (PSF), which is typically achieved by imaging a point object of sub-diffraction dimensions (e.g. fluorescent bead) in 3D, or alternatively, by measuring the wavefront leaving the exit pupil of the microscope [10] and calculating the 3D PSF through a Fourier transform. Any deviation from the ideal PSF indicates the presence of aberrations, an effect that is often easier to detect on the axial plane (Figure 1b).

The implementation of AO in microscopy depends on how image formation is attained in the specific microscopy modality. For example, in laser scanning microscopy (e.g. confocal and multiphoton microscopy), specimen-induced aberrations distort the wavefront of the excitation light and prevent the formation of a diffraction-limited focal spot (Figure 1). For multiphoton microscopes, where the signal is detected by a non-imaging detector (e.g. a photomultiplier tube), aberration correction is only needed for the excitation light. In a confocal microscope, aberration correction is implemented in both the excitation light (providing a diffraction-limited excitation confinement) and the fluorescence emission (ensuring the in-focus fluorescence passes through the confocal pinhole), which can be accomplished using the same wavefront correction device located in a common path. In a widefield microscope, aberration correction is usually only applied to the emitted fluorescence, which has to travel through the aberrating sample before image formation takes place on a camera.

The relatively recent progress of adaptive optical microscopy has mainly been due to the availability of compact deformable mirrors (DMs) and liquid-crystal spatial light modulators (SLMs) — the most common wavefront shaping devices used in adaptive optical microscopy — and the advancement of wavefront sensing and control schemes. DMs consist of a reflective membrane, either continuous or segmented, that can be actively controlled. The shape on the DM's surface determines the phase profile imparted to the light reflecting off it. Typical DMs used for adaptive optical microscopy consist of ~100s of actuators, have high bandwidths (typically >1 kHz), and their operation is independent of light polarization. Different coatings can be used to optimize the reflectivity of DMs over a wide wavelength range. SLMs, on the other hand, are made of 100 000s or even millions of liquid crystal

cells, each imparting a phase offset to the light impinging on it. The much larger number of pixels allows for the correction of more complex aberrations. In contrast to DMs, SLMs have slower refresh rates (~60–300 Hz), and they operate for a specific polarization and within a narrow wavelength range (~100s nm).

Adaptive optics methods in microscopy

The different implementations of AO in microscopy [4–7] mainly differ in how the aberration is measured, and are commonly classified into direct and indirect wavefront sensing methods.

Direct wavefront sensing

Direct wavefront sensing methods make use of a dedicated wavefront sensor, such as a Shack–Hartmann (SH) wavefront sensor, to directly measure wavefront aberrations (Figure 2). Such a scheme has been widely employed in ground-based telescopes [11] to measure and correct atmospheric aberrations, allowing the formation of high-quality images of astronomical objects.

In optical microscopy, a common direct wavefront sensing approach involves measuring the wavefront from a light-emitting point-like source generated via fluorescence excitation or back scattering of the excitation light [12••,13••,14–23]. Light from such a 'guide star' accumulates aberrations as it propagates through the sample and the instrument before reaching a SH sensor, consisting of a 2D array of lenses and a camera (Figure 2a). The local slope of each wavefront segment can be determined from the displacement of the focus of the corresponding light ray from its aberration-free position on a camera placed at the focal plane of the lenslet array (Figure 2b). By assuming a continuous wavefront, the phase offset of each segment can be calculated [24] and the wavefront reconstructed. This information is then used to control the wavefront shaping device in order to compensate for instrument-induced and sample-induced aberrations before image formation. Since wavefront aberration is obtained in a single measurement, direct sensing and correction can operate at high speed (e.g. milliseconds).

Accurate wavefront aberration measurements from such a direct wavefront sensing scheme are only possible when enough ballistic (unscattered) light reaches the wavefront sensor. As such, this method works well in cultured cells and transparent specimens.

Indirect wavefront sensing

Indirect wavefront sensing schemes, needing only a wavefront shaping device, are typically easier to implement into existing microscopes and can be readily used for scattering samples (Figure 3). One of several indirect methods, based on pupil-segmentation, relies on similar physical principles as SH wavefront sensors. By measuring lateral image shifts when different pupil subregions are sequentially illuminated, the local slope of each wavefront segment can be calculated [25]. The phase of each segment can then be obtained by direct interference measurements [26] or through reconstruction algorithms. By illuminating one pupil segment at a time, each image is taken under a lower NA with an enlarged focus. As a result, the images can contain contributions from structures originally beyond the excitation

volume under full-pupil illumination, making image shift measurements difficult in densely labeled samples. Alternatively, the entire pupil can be illuminated at all times [27], thus maintaining the full excitation NA and rendering this approach applicable to samples of arbitrary labeling density. Scanning one ray around the aberrated reference focus formed by the remaining rays while monitoring the variation of the signal strength reveals the additional tilt needed for maximal interference, ultimately yielding the local slope of this wavefront segment. To speed up the aberration measurement and improve the signal-to-noise ratio, gradients of multiple wavefront segments can be determined in parallel through frequency multiplexing [28••].

Another indirect approach, known as modal wavefront sensing, involves acquiring a series of images while intentionally distorting the wavefront by a known combination of orthogonal aberration modes (e.g. Zernike polynomials) using a wavefront shaping device. The wavefront is adjusted iteratively until a certain image metric is optimized, such as brightness or sharpness [31–34]. When the signals are bright and stable, genetic or hill-climbing algorithms have been employed to find the optimal correction [35–38]. In some cases, the metric is mathematically related to the amount of aberrations present, and a minimum of N + 1 measurements need to be carried out for determining N aberration modes [39–41].

A different wavefront correction approach, termed 'focus scanning holographic aberration probing' (F-SHARP), directly measures the amplitude and phase of the scattered electric field PSF via the interference of two excitation beams, allowing for fast wavefront correction of both aberrations and scattering at high resolution [30••]. Placing a wavefront shaping element at a Fourier plane to the image plane, the required correction pattern is the two-dimensional Fourier transform of the measured PSF of the scattered electric field.

Adaptive optical imaging improves morphological imaging of neurons *in vivo*

Visualizing biological structures and processes *in vivo* is one of the most important applications of optical microscopy, as it allows the study of biological systems in their natural state, and can provide information otherwise not attainable from *in vitro* preparations. In the following, we review a number of recent experimental realizations that illustrate how neurobiology has benefited from using adaptive optical microscopy to correct for brain-induced aberrations *in vivo*.

For morphological imaging of neurons, measuring and correcting for brain-induced optical aberrations, using either direct or indirect wavefront sensing methods, improves image quality and can allow individual synaptic terminals to be resolved at depth.

Using a fast direct wavefront sensing scheme ('Direct wavefront sensing' section) with two-photon excited visible-fluorescent guide stars, diffraction-limited two-photon imaging was demonstrated in large volumes (>240 μm per side) in zebrafish larval brains *in vivo* (Figure 2c) [12••]. This correction scheme was also applied for multicolor diffraction-limited confocal imaging in the zebrafish brain down to 200 μm, allowing for the study of subcellular organelles [12••]. By making use of the reduced tissue scattering of NIR guide

stars, the applicability of direct wavefront sensing was extended to tissues that strongly scatter visible light [13••]. Such an approach allowed *in vivo* two-photon microscopy imaging of the mouse brain at depth (Figure 2d), with the ability to resolve synaptic structures down to 760 μm.

To use the visible fluorescent signal for wavefront sensing in scattering brain tissue at depth, indirect wavefront sensing methods need to be employed. In one of the early demonstrations of adaptive optical microscopy for *in vivo* brain imaging, a pupil-segmentation approach with single-segment illumination ('Indirect wavefront sensing' section) allowed for diffraction-limited two-photon imaging 450 μm below the surface of the mouse brain *in vivo* [42•]. The same method has also been used to correct for system aberrations in two-photon fluorescence microendoscopy [43,44]. For more densely labeled samples, the frequency-multiplexed pupil-segmentation method ('Indirect wavefront sensing' section) proved successful at measuring and correcting for aberrations during *in vivo* two-photon imaging of *Caenorhabditis elegans*, zebrafish larva, and mouse brains [28••]. With the synaptic-level resolution achievable with such a scheme, it was possible to resolve submicrometer-sized spines inside a Thy1-YFP-H mouse brain at depth (Figure 3b). For a more densely labeled brain (wild-type mouse with viral GCaMP 6s [45] expression), a single correction improved image quality at 427-μm to 547-μm depth, with fine neuronal processes and even the much larger somata going from invisible to clearly resolvable after AO correction.

Other indirect wavefront sensing methods have also been used to improve the signal and contrast during *in vivo* brain imaging. Modal approaches have been used to improve image quality in two-photon imaging of the mouse brain *in vivo* [33,46]. Three-photon fluorescence microscopy, where longer excitation wavelengths lead to reduced light scattering and larger *in vivo* imaging depth [47,48], also benefits from AO correction [49]. A modal approach has been used to improve the signal and contrast during *in vivo* three-photon imaging of neurons (780 μm depth) and vasculature (1-mm depth) inside the mouse brain [50•]. The greater penetration depth of three-photon excitation also allowed transcuticle three-photon imaging of neuronal structures in the lateral horn of the fly brain, where a modal approach was used to correct the aberration introduced by the cuticle and the brain (Figure 3c) [29•]. F-SHARP [30••] ('Indirect wavefront sensing' section) can compensate for both aberrations and scattering, allowing the acquisition of high-contrast images inside turbid tissue, including zebrafish larva and mouse brain *in vivo* (Figure 3d).

Some general rules can be recognized from these studies.

Unlike the atmospheric aberration in astronomical AO, which changes on the scale of milliseconds and requires fast direct wavefront sensing for realtime correction, aberrations in the brain are much more temporally stable. Time-varying aberrations may arise, if brains in the embryo stage need to be imaged over hours, during which changes in the shape and/or composition of the brains may lead to variations in the brain-induced aberration. However, aberrations in the adult brains are usually temporally stable when compared to the imaging period [42•]. This makes the speed of aberration correction a less crucial factor and allows both direct and indirect wave-front sensing methods to achieve effective corrections.

The mouse brain has limited curvature (often further reduced by the cranial window that presses on the brain), which allows a single correction to improve image quality over hundreds of microns in 3D [13••,28••,42•]. The low spatiotemporal variation of brain-induced aberrations therefore facilitates the application of adaptive optical microscopy to mouse brains, where aberration correction only needs to be carried out at the beginning of an imaging session, with the resulting correction improving the image quality throughout the hours of experiments to follow.

In contrast, in highly curved samples such as zebrafish larval brain [13••] or *C. elegans* [28••], corrective patterns are often highly local, and a single aberration correction may improve image quality only in the close vicinity (tens of microns) of where the wavefront was measured. For such samples, direct wavefront sensing, if applicable, is the preferred choice due to its high correction speed.

In scattering tissue (e.g. adult brains), to compensate for the exponential loss of ballistic photons with imaging depth, one has to increase the excitation power exponentially. Eventually, the electric field strength at the surface of the brain becomes high enough to generate two-photon fluorescence signal without the need for focal confinement. When the out-of-focus fluorescence signal over-whelms the in-focus signal, the ultimate imaging depth limit of two-photon fluorescence microscopy is reached [51]. Because AO increases focal intensity and thus in-focus signal, but affects out-of-focus signal minimally [28••], correcting brain-induced aberrations increases the imaging depth limits.

One consistent observation is that correcting the same specimen-induced aberration improves the brightness of small features (e.g. synaptic terminals) more than large features (e.g. somata) [28••,42•]. This is because aberrations lead to an enlarged focal volume and thus weaker light intensity. The signal of small features approaching a point object, depends on local light intensity, and thus is substantially reduced by the focal intensity loss in an aberrated focus. For large extended features, on the other hand, the reduction of focal intensity is partly compensated by the increase of focal volume, which allows more fluorophores to contribute to the final signal [52]. In other words, while fluorescent probes and excitation strategies utilizing a longer wavelength range allow cell bodies to be visualized at increasing depths [48,53,54], adaptive optical microscopy remains crucially needed whenever synapse-sized structures are to be imaged at depth.

Adaptive optical imaging improves functional imaging of neurons *in vivo*

In the context of neurobiology, an important class of experiments involves measuring neural activity with fluorescent indicators, with the most popular being calcium transient measurements using genetically encoded calcium indicators such as GCaMP6 [45,55]. AO correction leads to a more accurate characterization of the functional properties of neurons.

Similar to morphological imaging, AO correction improves the brightness and contrast of functional images (Figure 4a). In addition, it has been consistently observed that the amplitude of calcium transients increases after AO correction [13••,28••,42•,56••], which results from the reduced excitation focal volume and enhanced focal brightness after

aberration correction. In brains densely labeled with fluorescent sensors (e.g. through bulk loading [42•], viral injection [28••], or transgenic expression [13••,46]) another challenge arises: in addition to the more brightly labeled neurons of interest (i.e. the ones from which regions of interest are chosen), there is also a spatially diffuse neuropil background from more weakly labeled neurons. Because this signal is an average from many neurons and is generally less correlated with the stimulus feature, it is considered a contamination [57]. As explained in the previous section, aberration correction increases the signal from our spatially confined regions of interest more than that from the neuropil contamination, and thus increases the strength of calcium transients.

For orientation tuning measurements that characterize the selectivity of neurons in the mouse visual pathway towards drifting gratings of various orientations, AO correction leads to a sharpening of their tuning curves (Figure 4). When imaging thalamic boutons located in the primary visual cortex of awake mice (Figure 4b), it was found that the percentage of visually responsive boutons, as well as those classified as orientation selective, steadily increases with decreasing amount of aberration [56••]: with a 340-μm-thick cranial window, 70% of all imaged boutons appeared to be non-responsive to visual stimuli and only 7% satisfied orientation-selective criteria; with a thinner cranial window of 170 μm, 31% of boutons were found to satisfy orientation-selective criteria, in contrast to 48% orientation-selective boutons as determined when the same boutons were imaged after AO correction. Between the latter two conditions, correcting aberrations sharpens the orientation tuning curves and leads to an overall shift of the global orientation selectivity index distribution towards higher selectivity, more accurately reflecting the tuning properties of these synaptic inputs.

Conclusions and future directions

Adaptive optical microscopy has proven successful at measuring and correcting for brain-induced aberrations at depth, providing the synaptic resolution required for accurate characterization of both structural and functional properties of neurons. Given the maturity of this methodology, the next challenge is to advance from the demonstration-of-principle experiments to daily applications in neurobiology laboratories. For this, we need methods that can provide aberration correction for a wide variety of specimens, in a fast and accurate fashion, which, once implemented, are robust and simple to use. Finding the best AO method to use, however, is complicated by several factors, including the spatial and temporal variabilities of the aberrations to be corrected, whether the sample is transparent or highly scattering, together with the available budget and expertise. Direct sensing methods outperform indirect methods when it comes to aberration measurement speed and accuracy, provided enough unscattered light reaches the SH wavefront sensor. Indirect methods are easier to implement into existing microscopes and work for both scattering and transparent samples, but can be slow and may not always reach optimal correction. Once implemented, however, emerging brighter and longer-wavelength fluorescent sensors would allow adaptive optical microscopy to push the depth limits of *in vivo* imaging in scattering samples even further.

Acknowledgments

References and recommended reading

Papers of particular interest, published within the period of review, have been highlighted as:

• of special interest

•• of outstanding interest

1. Mosk AP, Lagendijk A, Lerosey G, Fink M. Controlling waves in space and time for imaging and focusing in complex media. Nat Photonics. 2012; 6:283–292.

2. Horstmeyer R, Ruan H, Yang C. Guidestar-assisted wavefront-shaping methods for focusing light into biological tissue. Nat Photonics. 2015; 9:563–571. [PubMed: 27293480]

3. Vellekoop IM. Feedback-based wavefront shaping. Opt Express. 2015; 23:12189–12206. [PubMed: 25969306]

4. Kubby, JA. Adaptive Optics for Biological Imaging. Boca Raton, FL: CRC Press; 2013.

5. Booth MJ. Adaptive optical microscopy: the ongoing quest for a perfect image. Light Sci Appl. 2014; 3:e165.

6. Booth M, Andrade D, Burke D, Patton B, Zurauskas M. Aberrations and adaptive optics in super-resolution microscopy. Microscopy. 2015; 64:251–261. [PubMed: 26124194]

7. Ji N. Adaptive optical fluorescence microscopy. Nat Methods. 2017; 14:374–380. [PubMed: 28362438]

8. Schwertner M, Booth M, Wilson T. Characterizing specimen induced aberrations for high NA adaptive optical microscopy. Opt Express. 2004; 12:6540–6552. [PubMed: 19488305]

9. Schwertner M, Booth MJ, Neil MAA, Wilson T. Measurement of specimen-induced aberrations of biological samples using phase stepping interferometry. J Microsc. 2004; 213:11–19. [PubMed: 14678508]

10. Beverage JL, Shack RV, Descour MR. Measurement of the three-dimensional microscope point spread function using a Shack–Hartmann wavefront sensor. J Microsc. 2002; 205:61–75. [PubMed: 11856382]

11. Hardy, J. Adaptive Optics for Astronomical Telescopes. Oxford University Press; 1998.

12††. Wang K, Milkie DE, Saxena A, Engerer P, Misgeld T, Bronner ME, Mumm J, Betzig E. Rapid adaptive optical recovery of optimal resolution over large volumes. Nat Methods. 2014; 11:625–628. In this article, a direct wavefront sensing approach was used to measure and correct aberrations over large volumes within the zebrafish larval brain, at a measurement and correction rate of 14 ms. [PubMed: 24727653]

13††. Wang K, Sun W, Richie CT, Harvey BK, Betzig E, Ji N. Direct wavefront sensing for high-resolution in vivo imaging in scattering tissue. Nat Commun. 2015; 6:7276. By making use of the reduced tissue scattering of NIR guide stars, the authors extended the applicability of direct wavefront sensing to tissues that strongly scatter visible light. This allowed *in vivo* two-photon microscopy imaging of the mouse brain, with synaptic-level resolution, down to 760 μm. [PubMed: 26073070]

14. Azucena O, Crest J, Cao J, Sullivan W, Kner P, Gavel D, Dillon D, Olivier S, Kubby J. Wavefront aberration measurements and corrections through thick tissue using fluorescent microsphere reference beacons. Opt Express. 2010; 18:17521–17532. [PubMed: 20721137]

15. Azucena O, Crest J, Kotadia S, Sullivan W, Tao X, Reinig M, Gavel D, Olivier S, Kubby J. Adaptive optics wide-field microscopy using direct wavefront sensing. Opt Lett. 2011; 36:825–827. [PubMed: 21403697]

16. Jorand R, Le Corre G, Andilla J, Maandhui A, Frongia C, Lobjois V, Ducommun B, Lorenzo C. Deep and clear optical imaging of thick inhomogeneous samples. PLOS ONE. 2012; 7:e35795. [PubMed: 22558226]

17. Rueckel M, Mack-Bucher JA, Denk W. Adaptive wavefront correction in two-photon microscopy using coherence-gated wavefront sensing. Proc Natl Acad Sci U S A. 2006; 103:17137–17142. [PubMed: 17088565]

18. Cha JW, Ballesta J, So PTC. Shack–Hartmann wavefront-sensor-based adaptive optics system for multiphoton microscopy. J Biomed Opt. 2010; 15:046022. [PubMed: 20799824]

19. Aviles-Espinosa R, Andilla J, Porcar-Guezenec R, Olarte OE, Nieto M, Levecq X, Artigas D, Loza-Alvarez P. Measurement and correction of in vivo sample aberrations employing a nonlinear guide-star in two-photon excited fluorescence microscopy. Biomed Opt Express. 2011; 2:3135–3149. [PubMed: 22076274]

20. Tao X, Fernandez B, Azucena O, Fu M, Garcia D, Zuo Y, Chen DC, Kubby J. Adaptive optics confocal microscopy using direct wavefront sensing. Opt Lett. 2011; 36:1062–1064. [PubMed: 21478983]

21. Tao X, Azucena O, Fu M, Zuo Y, Chen DC, Kubby J. Adaptive optics microscopy with direct wavefront sensing using fluorescent protein guide stars. Opt Lett. 2011; 36:3389–3391. [PubMed: 21886220]

22. Rahman SA, Booth MJ. Direct wavefront sensing in adaptive optical microscopy using backscattered light. Appl Opt. 2013; 52:5523–5532. [PubMed: 23913074]

23. Tao X, Crest J, Kotadia S, Azucena O, Chen DC, Sullivan W, Kubby J. Live imaging using adaptive optics with fluorescent protein guide-stars. Opt Express. 2012; 20:15969–15982. [PubMed: 22772285]

24. Southwell W. Wave-front estimation from wave-front slope measurements. J Opt Soc Am. 1980; 70:998–1006.

25. Ji N, Milkie DE, Betzig E. Adaptive optics via pupil segmentation for high-resolution imaging in biological tissues. Nat Methods. 2010; 7:141–147. [PubMed: 20037592]

26. Liu R, Milkie DE, Kerlin A, MacLennan B, Ji N. Direct phase measurement in zonal wavefront reconstruction using multidither coherent optical adaptive technique. Opt Express. 2014; 22:1619–1628. [PubMed: 24515167]

27. Milkie DE, Betzig E, Ji N. Pupil-segmentation-based adaptive optical microscopy with full-pupil illumination. Opt Lett. 2011; 36:4206–4208. [PubMed: 22048366]

28††. Wang C, Liu R, Milkie DE, Sun W, Tan Z, Kerlin A, Chen T-W, Kim DS, Ji N. Multiplexed aberration measurement for deep tissue imaging in vivo. Nat Methods. 2014; 11:1037–1040. An indirect wavefront sensing approach, based on pupil segmentation using frequency multiplexing, was used to determine sample-induced aberrations in various model systems with arbitrary labeling density, and recover diffraction-limited imaging performance *in vivo*. With this approach it was possible to resolve submicrometer-sized spines deep within the highly scattering mouse brain, and drastically improve the detection of calcium transients at depth. [PubMed: 25128976]

29†. Tao X, Lin H-H, Lam T, Rodriguez R, Wang JW, Kubby J. Transcutical imaging with cellular and subcellular resolution. Biomed Opt Express. 2017; 8:1277–1289. In this study, a modal approach for wavefront correction is used to improve signal and contrast during transcutical three-photon imaging of the fly brain. [PubMed: 28663828]

30††. Papadopoulos IN, Jouhanneau J-S, Poulet JFA, Judkewitz B. Scattering compensation by focus scanning holographic aberration probing (F-SHARP). Nat Photonics. 2017; 11:116–123. In this article, an indirect wavefront sensing scheme was presented, which can compensate for both aberrations and scattering inside turbid media, by directly measuring the electric-field point spread function. This method proved successful at measuring and correcting for aberrations in zebrafish larvae and mouse brain *in vivo*.

31. Booth MJ. Wave front sensor-less adaptive optics: a model-based approach using sphere packings. Opt Express. 2006; 14:1339–1352. [PubMed: 19503457]

32. Débarre D, Booth MJ, Wilson T. Image based adaptive optics through optimisation of low spatial frequencies. Opt Express. 2007; 15:8176–8190. [PubMed: 19547145]

33. Galwaduge PT, Kim SH, Grosberg LE, Hillman EMC. Simple wavefront correction framework for two-photon microscopy of in-vivo brain. Biomed Opt Express. 2015; 6:2997–3013. [PubMed: 26309763]

34. Zeng J, Mahou P, Schanne-Klein M-C, Beaurepaire E, Débarre D. 3d resolved mapping of optical aberrations in thick tissues. Biomed Opt Express. 2012; 3:1898–1913. [PubMed: 22876353]

35. Albert O, Sherman L, Mourou G, Norris TB, Vdovin G. Smart microscope: an adaptive optics learning system for aberration correction in multiphoton confocal microscopy. Opt Lett. 2000; 25:52–54. [PubMed: 18059779]

36. Sherman L, Ye JY, Albert O, Norris TB. Adaptive correction of depth-induced aberrations in multiphoton scanning microscopy using a deformable mirror. J Microsc. 2002; 206:65–71. [PubMed: 12000564]

37. Marsh PN, Burns D, Girkin JM. Practical implementation of adaptive optics in multiphoton microscopy. Opt Express. 2003; 11:1123–1130. [PubMed: 19465977]

38. Wright AJ, Burns D, Patterson BA, Poland SP, Valentine GJ, Girkin JM. Exploration of the optimisation algorithms used in the implementation of adaptive optics in confocal and multiphoton microscopy. Microsc Res Tech. 2005; 67:36–44. [PubMed: 16025475]

39. Booth MJ, Neil MAA, Jukaitis R, Wilson T. Adaptive aberration correction in a confocal microscope. Proc Natl Acad Sci U S A. 2002; 99:5788–5792. [PubMed: 11959908]

40. Booth MJ. Wavefront sensorless adaptive optics for large aberrations. Opt Lett. 2007; 32:5–7. [PubMed: 17167565]

41. Débarre D, Botcherby EJ, Booth MJ, Wilson T. Adaptive optics for structured illumination microscopy. Opt Express. 2008; 16:9290–9305. [PubMed: 18575493]

42†. Ji N, Sato TR, Betzig E. Characterization and adaptive optical correction of aberrations during in vivo imaging in the mouse cortex. Proc Natl Acad Sci U S A. 2012; 109:22–27. In this article, the authors demonstrated the use of adaptive optical microscopy for *in vivo* brain imaging, using a pupil-segmentation approach with single-segment illumination. Diffraction-limited two-photon imaging was achieved 450 μm inside the mouse brain. [PubMed: 22190489]

43. Wang C, Ji N. Pupil-segmentation-based adaptive optical correction of a high-numerical-aperture gradient refractive index lens for two-photon fluorescence endoscopy. Opt Lett. 2012; 37:2001–2003. [PubMed: 22660101]

44. Wang C, Ji N. Characterization and improvement of three-dimensional imaging performance of grin-lens-based two-photon fluorescence endomicroscopes with adaptive optics. Opt Express. 2013; 21:27142–27154. [PubMed: 24216938]

45. Chen T-W, Wardill TJ, Sun Y, Pulver SR, Renninger SL, Baohan A, Schreiter ER, Kerr RA, Orger MB, Jayaraman V, Looger LL, Svoboda K, Kim DS. Ultrasensitive fluorescent proteins for imaging neuronal activity. Nature. 2013; 499:295–300. [PubMed: 23868258]

46. Park J-H, Kong L, Zhou Y, Cui M. Large-field-of-view imaging by multi-pupil adaptive optics. Nat Methods. 2017; 14:581–583. [PubMed: 28481364]

47. Horton NG, Wang K, Kobat D, Clark CG, Wise FW, Schaffer CB, Xu C. In vivo three-photon microscopy of subcortical structures within an intact mouse brain. Nat Photonics. 2013; 7:205–209.

48. Ouzounov DG, Wang T, Wang M, Feng DD, Horton NG, Cruz-Hernandez JC, Cheng Y-T, Reimer J, Tolias AS, Nishimura N, Xu C. In vivo three-photon imaging of activity of GCaMP6-labeled neurons deep in intact mouse brain. Nat Methods. 2017; 14:388–390. [PubMed: 28218900]

49. Sinefeld D, Paudel HP, Ouzounov DG, Bifano TG, Xu C. Adaptive optics in multiphoton microscopy: comparison of two, three and four photon fluorescence. Opt Express. 2015; 23:31472–31483. [PubMed: 26698772]

50†. Sinefeld D, Paudel HP, Wang T, Wang M, Ouzounov DG, Bifano TG, Xu C. Nonlinear adaptive optics: aberration correction in three photon fluorescence microscopy for mouse brain imaging. Proc SPIE. 2017; 10073 1007314-1-1007314-7. A modal approach for wavefront correction is used to improve the signal and contrast during *in vivo* three-photon imaging of neurons (780 μm depth) and vasculature (1-mm depth) inside the mouse brain *in vivo*.

51†. Theer P, Hasan MT, Denk W. Two-photon imaging to a depth of 1000 mm in living brains by use of a Ti:Al$_2$O$_3$ regenerative amplifier. Opt Lett. 2003; 28:1022–1024. [PubMed: 12836766]

52. Xu, C., Webb, WW. Topics in Fluorescence Spectroscopy. Springer; 1997.

53. Dana H, Mohar B, Sun Y, Narayan S, Gordus A, Hasseman JP, Tsegaye G, Holt GT, Hu A, Walpita D, Patel R, Macklin JJ, Bargmann CI, Ahrens MB, Schreiter ER, Jayaraman V, Looger LL, Svoboda K, Kim DS. Sensitive red protein calcium indicators for imaging neural activity. eLife. 2016; 5:e12727. [PubMed: 27011354]

54. Kondo M, Kobayashi K, Ohkura M, Nakai J, Matsuzaki M. Two-photon calcium imaging of the medial prefrontal cortex and hippocampus without cortical invasion. eLife. 2017; 6:e26839. [PubMed: 28945191]

55. Yang W, Yuste R. In vivo imaging of neural activity. Nat Methods. 2017; 14:349–359. [PubMed: 28362436]

56††. Sun W, Tan Z, Mensh BD, Ji N. Thalamus provides layer 4 of primary visual cortex with orientation- and direction-tuned inputs. Nat Neurosci. 2016; 19:308–315. In this study, the authors examined the orientation tuning properties of thalamic boutons in the primary visual cortex of awake mice. The use of adaptive optical imaging — using an indirect wavefront sensing approach based on pupil segmentation — was found to be essential for accurate tuning curve characterization. [PubMed: 26691829]

57. Göbel W, Helmchen F. In vivo calcium imaging of neural network function. Physiology. 2007; 22:358. [PubMed: 18073408]
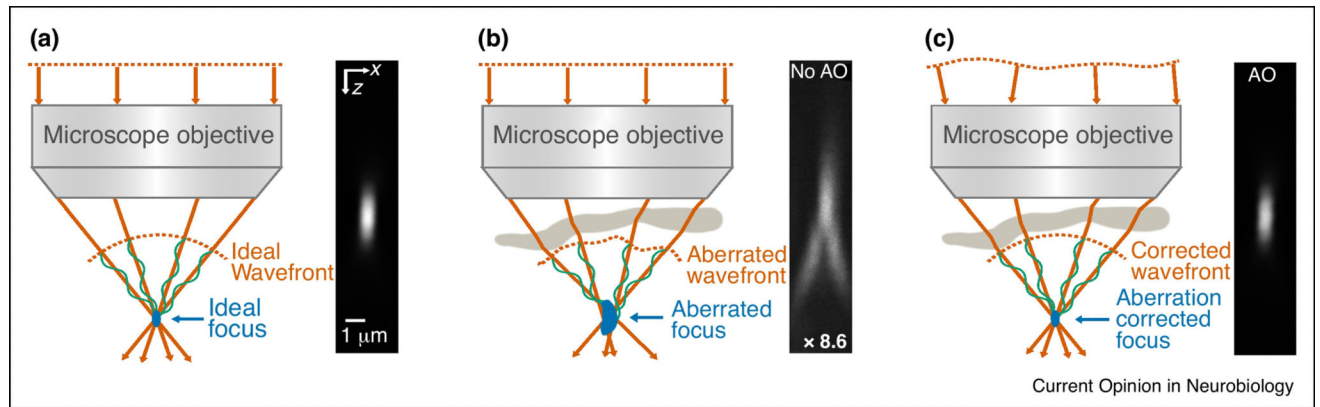
Figure 1.

The effect of aberrations on image quality. **(a)** An aberration-free wavefront leads to a diffraction-limited focal spot in a point-scanning (e.g. two-photon fluorescence) microscope. **(b)** Specimen refractive index mismatches distort the wavefront of the excitation light, leading to a dim, enlarged focus. **(c)** Optimal imaging performance can be recovered by pre-shaping the wavefront of the excitation light to cancel out the specimen-induced aberration. The sinusoidal curves denote the phase relationship among the rays. Axial images obtained from two-photon excitation of 1-µm fluorescent red beads are shown for three different cases: (a) ideal, aberration-free imaging conditions, (b) an artificial aberration is introduced, causing a 8.6-fold decrease in brightness and a degradation of axial resolution, and (c) adaptive optics is used to recover ideal imaging performance.
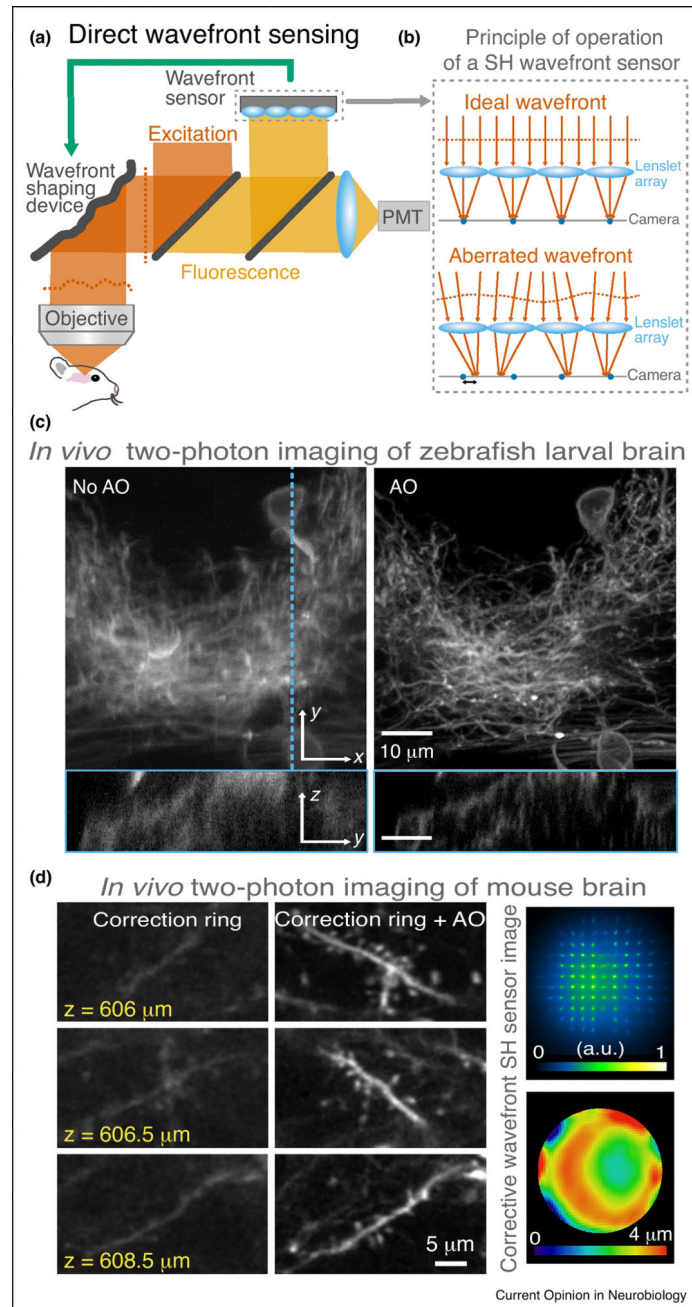
Figure 2.

Adaptive optical microscopy using direct wavefront sensing. **(a)** Two-photon fluorescence microscope using a Shack–Hartmann (SH) sensor. PMT, photomultiplier tube. **(b)** A wavefront is incident on a SH wavefront sensor, where an array of lenslets focus the light into a 2D array of foci onto a camera. The local slopes of wavefront segments can be measured from the displacements of the foci relative to their aberration-free positions. **(c)** Two-photon *in vivo* imaging of zebrafish larval brain obtained without and with AO correction [12••]. **(d)** Two-photon *in vivo* imaging of dendritic spines in the mouse brain

obtained without and with AO correction (left), and SH sensor image with its corresponding corrective wavefront (right) [13••].
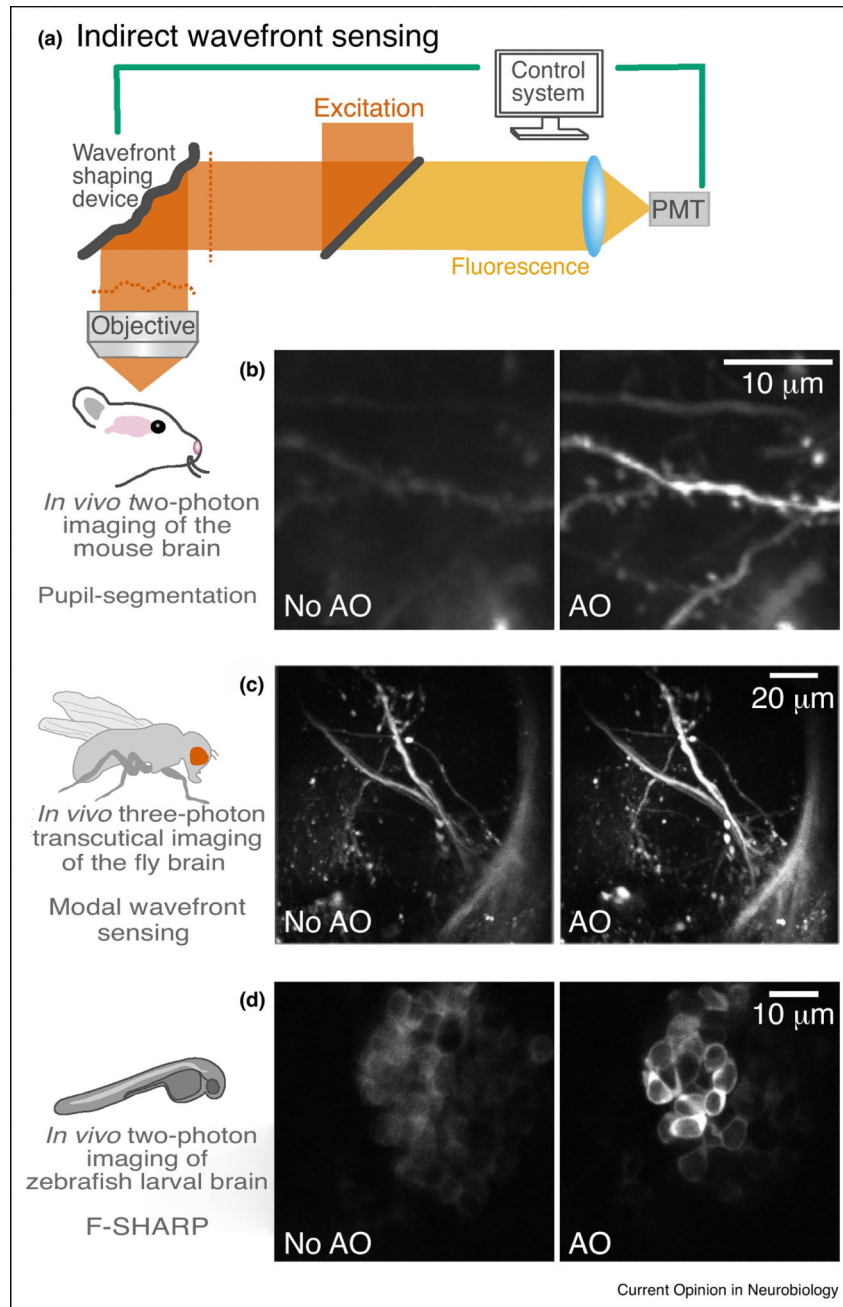
Figure 3.
Adaptive optical microscopy using indirect wavefront sensing. **(a)** An AO two-photon fluorescence microscope. PMT, photomultiplier tube. **(b)** Two-photon maximal-intensity projection images of dendrites at 376–395 μm below dura measured without and with AO in the mouse brain *in vivo*, using the frequency-multiplexed pupil-segmentation method [28••]. **(c)** *In vivo* three-photon transcutical imaging in the lateral horn of the fly brain [29•]. **(d)** Two-photon *in vivo* imaging of zebrafish larval brain obtained without and with AO correction, 300 μm under the brain surface, using F-SHARP [30••].
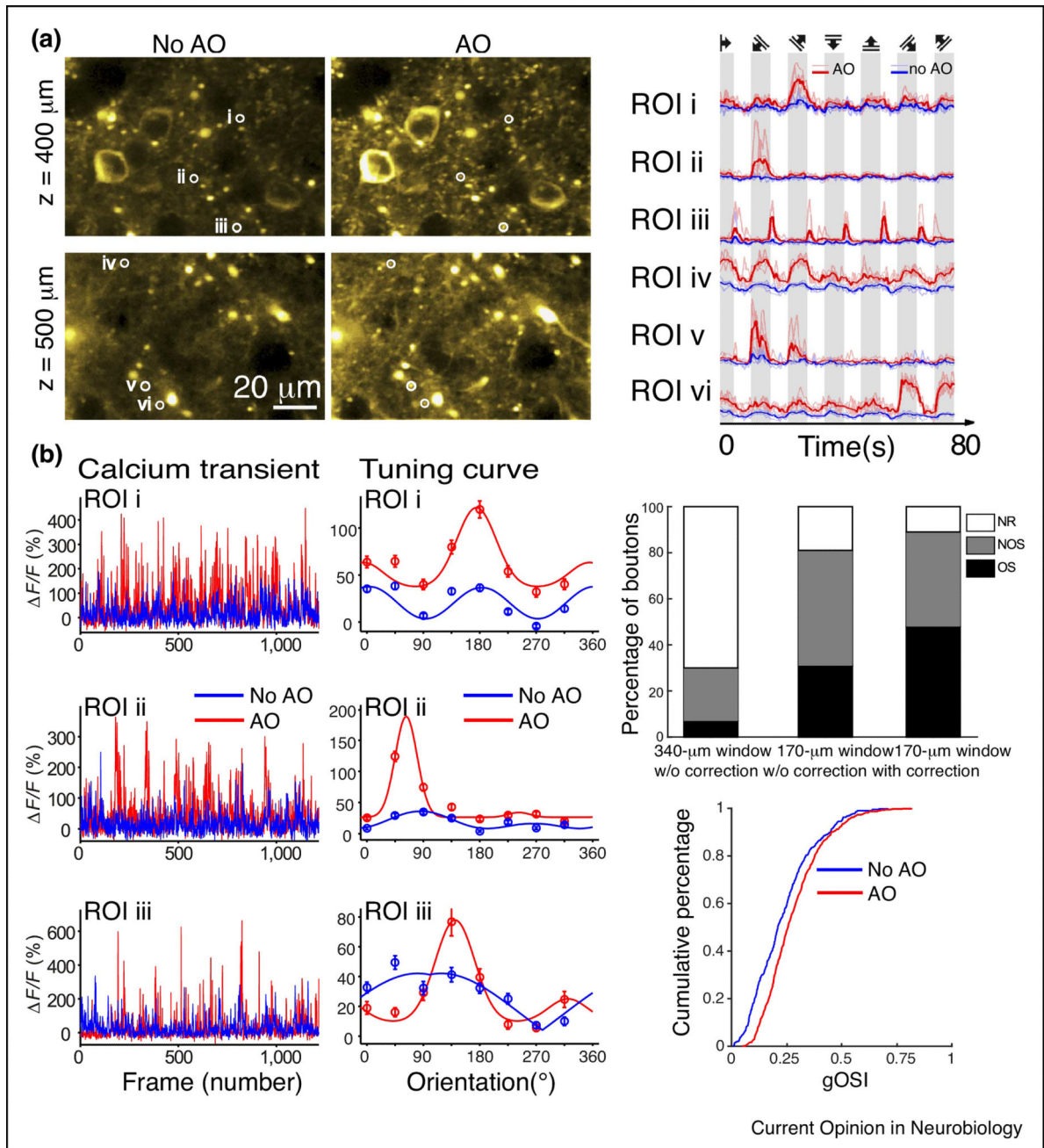
Figure 4.
Adaptive optics improves the accuracy of calcium activity measurements. **(a)** Calcium transients evoked by the stimulation of a drifting grating, 400 and 500 μm below pia in the primary visual cortex of a mouse (Thy1-GCaMP6s line GP4.3) without and with AO correction (left panel). Calcium transients at regions of interest (ROI) i–vi, without and with AO correction (right panel). **(b)** Calcium transients (left panel) and tuning curves (center panel) for three different ROIs taken from images of GCaMP6s+ thalamic axons without and with AO, at a depth of 170 μm. Percentages of non-responsive (NR), not orientation selective (NOS), and orientation selective (OS) boutons; and cumulative distributions of

global orientation selectivity index (gOSI) for boutons measured without and with AO (right panel). Cranial window thickness is 170 μm.